



Title	Three Dimensional Ceramics Printing to Create Ordered Dendrite Structures for Energy and Material Flows Modulation
Author(s)	Kirihara, Soshu
Citation	Transactions of JWRI. 2015, 44(2), p. 13-18
Version Type	VoR
URL	https://doi.org/10.18910/57268
rights	
Note	

The University of Osaka Institutional Knowledge Archive : OUKA

<https://ir.library.osaka-u.ac.jp/>

The University of Osaka

Three Dimensional Ceramics Printing to Create Ordered Dendrite Structures for Energy and Material Flows Modulation[†]

KIRIHARA Soshu *

Abstract

Ceramics dendrite structures with geometrically ordered lattices had been created successfully by using a laser scanning and micro patterning stereolithography. Micro rods of alumina, zirconia, titania and hidroxiapatite were connected to realize coordination numbers of four, six, eight and twelve for fluctuation modulations of electromagnetic wave, electronic current propagation, heat diffusion, stress distribution, liquid flow and gas dispersion. Intensity profiles of these energy fields and material densities were visualized theoretically though finite element methods to compare with measured results. Technological concepts of these ceramics dendrites can be applied to novel censor devices, composite materials, solid electrodes and biological implants in the near future. In this paper, fabrication processes of ceramic dendrites and numerical simulations of spatial gas flows, electromagnetic wave propagations and biological fluid flows will be discussed for novel energy production devices and biocompatible implants.

KEY WORDS: (Ceramics dendrite), (Solid electrolyte), (Dielectric material), (Biological scaffold), (Stereolithography), (Finite element method)

1. Introduction

For sustainable development and reduction of carbon dioxide emissions, solid oxide fuel cells (SOFCs) are investigated as novel generation systems of electric power with high efficiencies. Yttria stabilized zirconia (YSZ) with high ion conductivities for incident oxygen is widely adopted material for solid electrolyte anodes in the SOFC components [1]. Recently, porous network structures were introduced into YSZ electrodes in micrometer or nanometer sizes to increase the surface areas of the reaction interfaces. In this investigation, solid electrolyte dendrites composed of YSZ spatial lattice structures with various coordination numbers were fabricated successfully by using micro pattern stereolithography and nanoparticle sintering techniques. In these dendrite structures, stress distributions and fluid flows were simulated and visualized by using finite element methods. These new computer aided design, manufacture and evaluation (CAD/CAM/CAE) have been investigated to create micro components of various ceramic materials [2,3].

Novel electromagnetic devices were created. Photonic crystals with periodic arrangements of dielectric media can reflect the electromagnetic wave perfectly and can exhibit forbidden gaps in transmission spectra through Bragg diffraction [4,5]. Through introductions of air cavities into the periodic lattices, the electromagnetic

waves having specific wavelengths can resonate with structural defects, and localized modes of transmission peaks appear in the photonic band gap. Such localization function of electromagnetic waves can be applied to various devices, for example resonators, waveguides, and antennas. The photonic crystals with a diamond structure composed of alumina lattices were fabricated by using the micro patterning stereolithography. The artificial crystals can reflect the electromagnetic waves perfectly and prohibit the propagations for all directions in terahertz frequency range. The twinned diamond lattice structures including the plane defect were created to resonate with the terahertz waves and localize the electromagnetic energies for directional emissions. The terahertz waves are expected to detect micro cracks in material surfaces and structural defects in electric circuits by fine wave interferences, and to analyze cancer cells in human skins and toxic bacteria in natural foods through the higher frequency excitations. The electromagnetic wave transmissions were measured by using a terahertz wave spectroscopy. The resonance and diffraction behaviors were visualized and analyzed by a transmission line modeling method of a finite difference time domain simulations.

Tissue scaffolds are required to repair bone defects resulting from illnesses. To encourage osteoconductivity

[†] Received on November 27, 2015

* Associate Professor

Transactions of JWRI is published by Joining and Welding Research Institute, Osaka University, Ibaraki, Osaka 567-0047, Japan

3D Ceramics Printing to Create Ordered Dendrite Structures for Energy and Material Flows Modulation

and tissue regeneration, prosthetics to mimic bone porosity and optimized flow behavior are very important. Various techniques to fabricate the artificial bone structures have been investigated, for example, polycaprolactone scaffolds with variable pore size and porosity from 63 to 79% by using selective laser sintering, the modified hydroxyl apatite ones by printing process, and the periodic micro arrays by using direct ink writing. The scaffold structure requires suitable porosity and pore size to foster tissue regeneration in the human body [6]. The natural bone with graded porosity from 50 to 90 % in volume fraction is mimicked in fabrication of the artificial ones. However, the conventional common artificial bones have nearly 75% in porosity. In this investigation, creation of the novel artificial bones composed of hydroxyapatite ceramics with effective bio-compatibility and high mechanical strength will be demonstrated, and the graded porous structures composed of four coordinate lattices by using the laser scanning stereolithography. Evaluating osteogenesis requires long term clinical experiments. As an alternative to clinical experiments, the biological fluid flow behavior in different types of scaffold structures is examined.

2. Experimental procedure

The solid electrolyte dendrites with spatial lattice structures were designed by using a computer graphic application. These surface areas of reaction interfaces and the gap volume of stream paths were calculated geometrically for the dendrite lattice with four coordination numbers as shown in Fig. 1. The dendrite lattices of 1.16 in aspect ratio can be considered to exhibit the higher reaction efficiencies and gas transmittances according to Nernst equation. In the optimized dendrite structure, the diameter and length of YSZ rods were decided 92 and 107 μm , respectively. The lattice constant was 250 μm . The graphic data was converted into a stereolithographic format through polyhedral approximations. The solid model was sliced into the cross sectional numerical data sets to input the stereolithographic equipment (D-MEC: SI-C1000, Japan). Photo sensitive acrylic resin dispersed with YSZ particles of 60 and 100 nm in first and second diameters at 30 volume % were fed over a substrate from a dispenser nozzle. The highly viscous resin paste was fed with controlled air pressure, and spread uniformly by a mechanical knife edge. The thickness of each layer was controlled to 10 μm . The cross sectional pattern was formed through illuminating visible laser of 405 nm in wavelength on the resin surface. The high resolution image could be achieved by applying a digital micro mirror device (DMD) and an objective optical lens. Figure 2 shows a schematic illustration of the micro patterning stereolithography system. The DMD is an optical element assembled by micro mirrors of 14 μm in edge length. The tilting of each tiny mirror can be controlled according to the cross sectional data transferred from a computer. The solid micro structures were built by stacking these patterns layer by layer. In order to avoid deformation and cracking during dewaxing, careful investigations for the

heat treatment processes were required. The formed precursors with dendrite structures were heated at various temperatures from 100 to 600 $^{\circ}\text{C}$ while the heating rate was 1.0 $^{\circ}\text{C}/\text{min}$. The dewaxing process was observed in respect to the weight and color changes. The YSZ particles could be sintered at 1500 $^{\circ}\text{C}$ for 2 hs. The heating rate was 8.0 $^{\circ}\text{C}/\text{min}$. The density of the sintered sample was measured by using Archimedes method. The ceramic microstructures were observed by a digital optical microscope and scanning electron microscopy. In the lattice dendrites, fluid flow velocities and pressure stress distributions were simulated and visualized by a finite volume method (FVM) application.

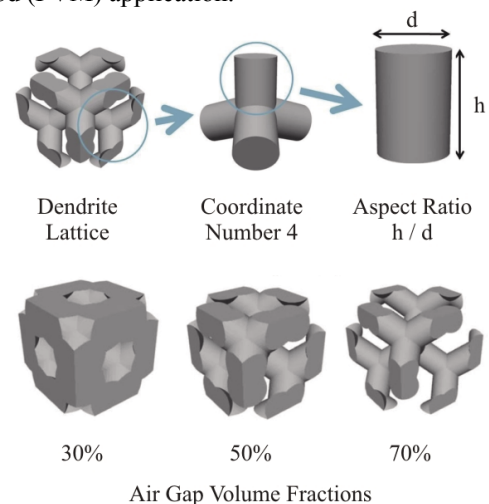


Fig. 1 Computer graphics of lattice distributions of dendrite structures with coordination number 4. Air gap volume fractions are changed with aspect ratios.

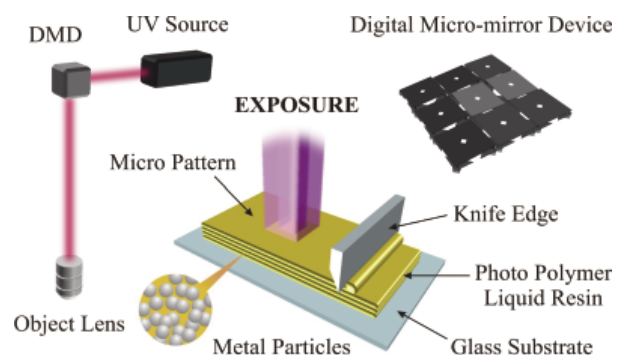


Fig. 2 Schematic illustrations of micro patterning stereo-lithography system. Two dimensional cross sectional layers are stacked up to create three di-mensional structures automatically.

Subsequently, the photonic crystals with diamond lattices composed of the alumina were fabricated by using the same methods. The whole structure was 6 \times 6 \times 2 mm in size consisting of 6 \times 6 \times 2 unit cells. The aspect ratio of the dielectric lattices was designed to be 1.5. The crystal structure was designed to open the perfect band

gap as shown in Fig. 3. Acryl precursors including alumina particles of 170nm at 40 volume % were heated at various temperatures from 100 to 600 °C while the heating rate was 1.0 °C/min. Nanometer sized alumina particles could be sintered at 1500 °C. The heating rate was 8.0 °C/min. The transmittance and the phase shift of incident terahertz waves were measured by using terahertz time domain spectroscopy (J-Spec 2001: Advanced Infrared Spectroscopy, Japan). Electric field intensities were simulated by a transmission line modeling (TLM) program.

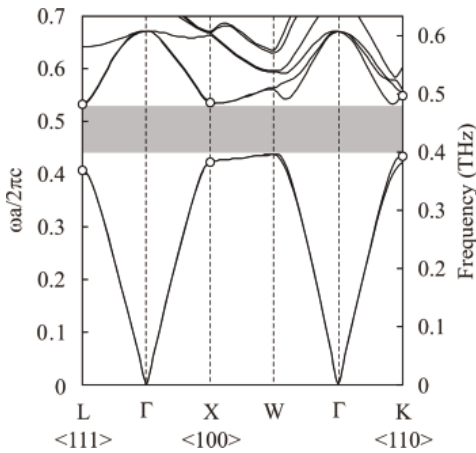


Fig. 3 A photonic band diagram calculated by the plane wave expansion method. Opened circles are measured edge frequencies of photonic band gaps. The dielectric constant of the lattice was 10. The frequency range with gray color indicates the perfect band gap in common for all directions.

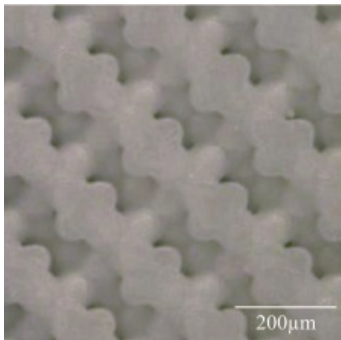


Fig. 4 Dendrite lattices of YSZ solid electrolyte processed by using the micro stereolithography and the nanoparticles sintering techniques successfully.

Moreover, the dendritic lattice structures in the biological scaffolds with 4, 6, 8 and 12 coordination numbers are designed. The porosity of scaffold models can be controlled in the range from 50 to 90 % by adjusting aspects ratios of the rod length to diameter. The porosity of all skeletal structures was 75%. This is the same value as the porosity of a human bone. These scaffolds have perfect interconnected pores. Fluid circulation in the various

dendrite scaffolds was visualized with the fluid dynamic solver. Flow velocity in the spatial grids in the scaffold models was calculated through the finite element method. The following values of these parameters were used in this simulation [7]. The fluid phase was represented as an incompressible Newtonian fluid with a viscosity of 1.45×10^{-3} Pa·s. The inlet velocity applied to the scaffolds was constant at 0.235 mm/s, and the pressure was zero at the outlet. No-slip surface conditions were assumed. Micron scale ceramic lattices have been successfully fabricated by the laser scanning stereolithography. Photo sensitive acrylic resin including the hydroxyapatite particles of 10 μ m in diameter at 45 volume % was used. The porosity of the scaffold form was approximately 75 %. The part accuracies of the lattices were measured under 50 μ m in size difference. The formed precursor was dewaxed at 600 °C for 2 hs with heating rate of 1.0 °C/min and sintered at 1250 °C for 2 hs with the rate of 5 °C/min in the air. The relative density of the sintered hydroxyapatite lattice was measured at 98 % by Archimedian method.

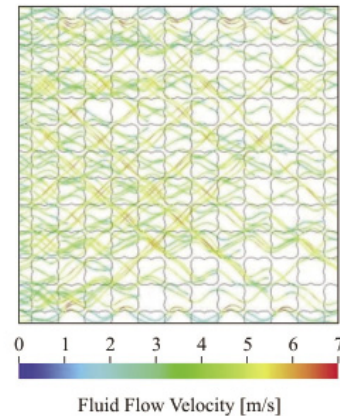


Fig. 5 A distribution of fluid flow velocities in the dendrite lattice structure simulated and visualized by using a FVM method. The curved lines show the fluid flow paths according to the velocity vectors.

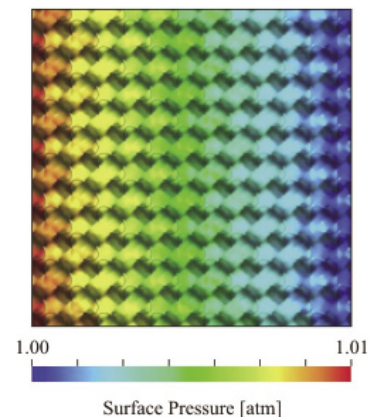


Fig. 6 The distribution of the surface pressure on the ceramics lattice of dendrite structure. The red and blue areas show the higher and lower gas pressures on the reaction interfaces, respectively.

3D Ceramics Printing to Create Ordered Dendrite Structures for Energy and Material Flows Modulation

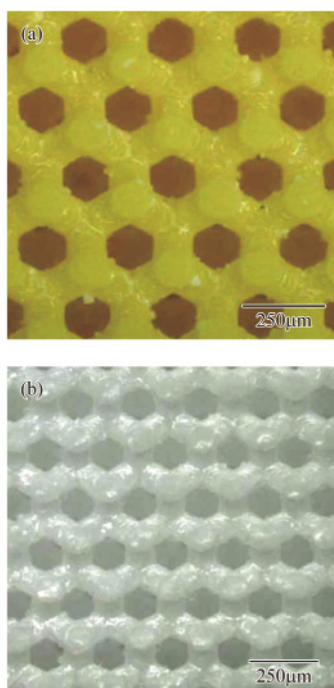


Fig. 7 Diamond photonic crystals formed by the stereolithography (a) and sintered one (b).

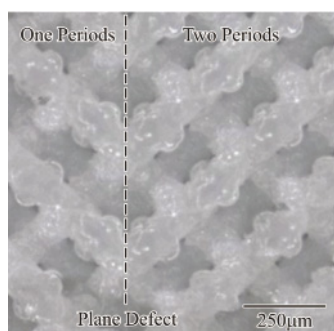


Fig. 8 A modified diamond photonic crystal with a plane defect between twinned lattice structures.

3. Results and Discussion

The sintered solid electrolyte dendrite with the YSZ micro lattice structure is shown in Fig. 4. Deformation and cracking are not observed. The volume fraction of the air gaps was 50 % by the open paths. In previous investigations, the porous electrodes were formed by sintering the YSZ surly with polystyrene particles dispersion. Therefore, it is difficult to realize the prefect opened pores structures with the higher porosity over 40 % in volume fraction. In the dense microstructure of the YSZ lattice, the average grain size was approximately 4 μm . The relative density reached at 95 %. Micrometer sized cracks or pores were not observed. The obtained dense YSZ lattice structure will exhibit higher performances in mechanical properties than the porous electrodes of the solid electrolyte dendrites. The fluid flow velocities were

visualized by using the FVM method as shown in Fig. 5. All air paths were opened for outsides and connected with each other in the YSZ dendrite lattice structures. The fluid flows can transmit in the one direction smoothly. The pressure stress distributions in the dendrite were visualized as shown in Fig. 6. The fluid pressures were gradually distributed for flow direction, and the localization of the stress was not observed. The fabricated solid electrolyte dendrites with YSZ lattices can be considered to have higher performances as novel ceramic electrodes.

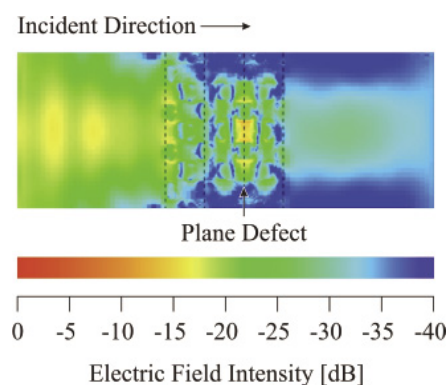


Fig. 9 A cross sectional images of electric field intensity in the twinned diamond photonic crystal.

The diamond structures formed by micro stereolithography and in the sintered alumina lattice are shown in Fig. 7-(a) and (b). The micron size order dielectric pattern was created successfully according the geometrical design. The micro clacks or pores were not observed in the microstructure observations. The part accuracy of sintered sample was reacted at $\pm 10\mu\text{m}$ comparing with the designed structure. Through the computer aided design and manufacture processes, the twinned diamond lattice was fabricated as shown in Fig. 8. These mirror symmetric diamond lattices were formed with high part accuracies. The lattice constant of the diamond structure is 375 μm . The relative density reached 97.5 %. The measured band gap frequencies were compared with calculation results by the TLM method. The measured frequency ranges of opaque regions corresponded to the calculation. The complete photonic band gap opened between 0.40 and 0.47 THz. Two and three period lattice structures were arranged on the right and left side of the plane defect, respectively. A terahertz wave was transmitted from left to right. In the measured transmission spectrum, one localized mode peak was observed in the band gap at the frequencies of 0.42 THz. The measured band gap region and the peak frequency of the localized mode were compared with calculations by the TLM method. They were in good agreement. The electric field distribution in the twinned diamond lattices was simulated as shown in Fig. 9. Incident terahertz wave was resonate and localized in the plane defect region between the twinned diamond lattices. The amplified electromagnetic wave by multiple reflections can transmit through the photonic crystal. Therefore, the transmission peak will be

formed in the band gap. On the right side of the sample, the radiation pattern showed the plane wave expansion. The micro photonic crystal with the twinned ceramic lattice of the diamond structure can be applied to a terahertz beam emitters.

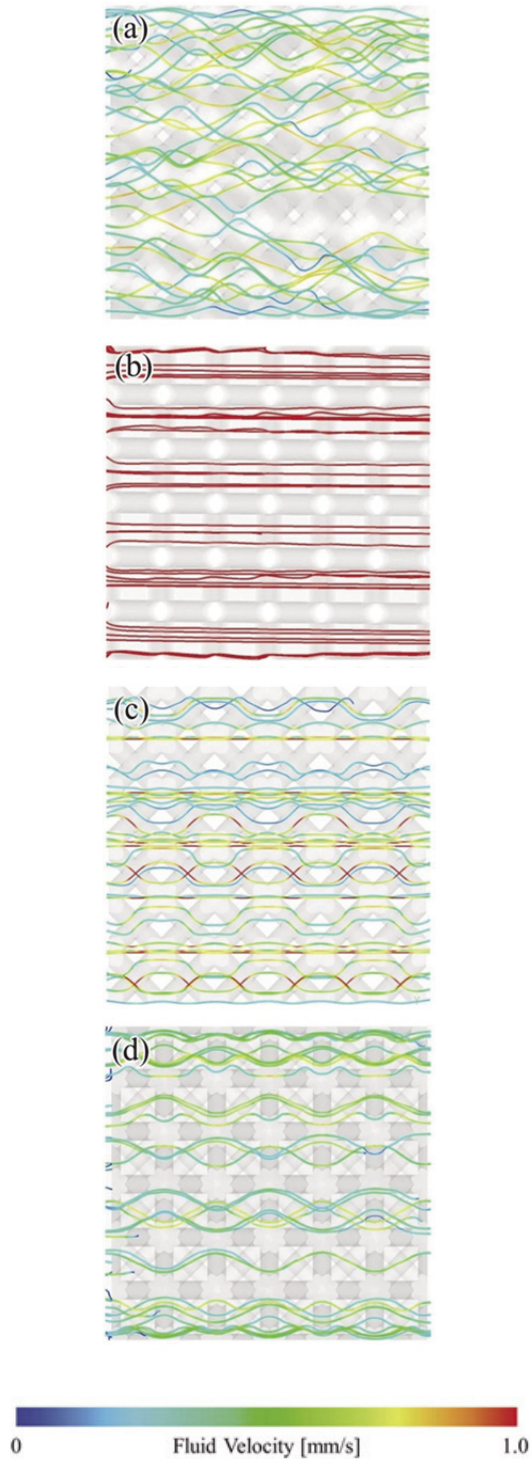


Fig. 10 Fluid flow behaviors in the dendrite scaffolds visualized using the finite element method.

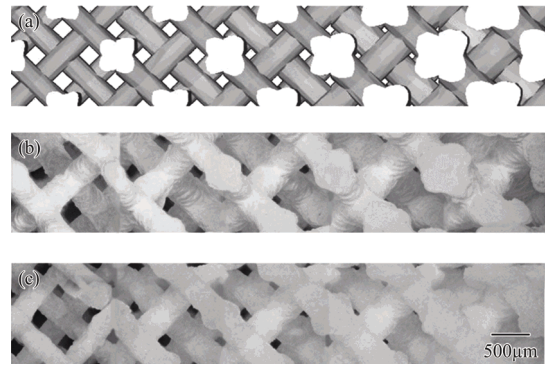


Fig. 11 Four-coordinate lattices with the graded porous structures. (a) the designed computer graphic model, (b) the acrylic lattices including hydroxylapatite particles fabricated by the stereolithography, (c) the sintered ceramic scaffold.

Streamline behavior in the dendrite scaffolds are shown in Fig. 10. Figure 10-(a) shows a 4 coordinate scaffold structure and indicates that inordinate flow at a low velocity was obtained. This also indicates simulated biological fluid flow to the whole structure, which is expected to provide active tissue regeneration. The fluid velocity in the scaffolds of coordination number 6 is the highest at above 1.0 mm/s as shown in Fig. 10-(b). There are no blockades from the inlet to the outlet, and the flow becomes linearly stable. The high fluid velocity area above 1.0 mm/s in the scaffold is subjected to shear stress which can assume the difficulty cell attachment on the scaffolds surface. In the case of 8 coordination number scaffold, random fluid flow and high velocity are exhibited in some parts of the structure as shown in Fig. 10-(c). Smooth fluid flows and propagations are visualized in the 4 coordination number scaffold without obstacles lattices comparing with the larger numbers rod coordination. In the structure of coordination number 12, moderate velocities and flow behaviors are exhibited as shown in Fig. 10-(d). However, there are no active flows in some areas because of many rods in the architecture. The designed scaffold model with the graded porous structure is shown in Fig. 11. The porosity is distributed gradually through modulations of the aspect ratio in the 4 coordination number lattices as shown in Fig. 11-(a). The acrylic scaffolds with hydroxyapatite particles is shown in Fig. 11-(b). The sintered scaffold model of the hydroxyapatite ceramic with the graded lattices is shown in Fig. 11-(c). The linear shrinkage ratios for horizontal and vertical axis were 23 and 25 %, respectively. The smaller lattice structures could be obtained effectively through the controlled body shrinkages on the optimized sintering process. The microstructure of the sintered scaffold is observed by the scanning electron microscope. Cracks and pores were not observed. The grain size is about 4 μm . The relative density reached at 98 %. The formed scaffold is considered to perform the effective biocompatibility and high mechanical strength.

3D Ceramics Printing to Create Ordered Dendrite Structures for Energy and Material Flows Modulation

4. Summary

We have fabricated solid electrolyte dendrites with yttria stabilized zirconia lattices for anode electrodes of solid oxide fuel cells. Acryl precursors including ceramic particles were formed successfully by using micro patterning stereolithography. Thorough careful optimization of process parameters in dewaxing and sintering, we have succeeded in fabricating dense ceramic micro components. These solid electrolyte dendrites with opened air path networks exhibited effective transmission properties of fluid flows. These novel ceramic electrodes have the potential to contribute to developments of compact fuel cells. Subsequently, alumina photonic crystals with a diamond structure of spatially periodic arrangement were created with high part accuracies by using stereolithography and sintering. The diamond lattice can open a perfect photonic band gap. Twinned dielectric lattices including plane defect can realize directional emission of electromagnetic waves with terahertz frequency. These formed micro devices will be applied for sensor heads to detect harmful materials in the air or water of environmental fields. Moreover, hydroxyapatite artificial bones with graded porous structures composed of 4 coordinate lattices were created by stereolithography and sintering. The micro porous structures were optimized by fluid flow simulations. In the microstructure of sintered scaffold, cracks and pores were not observed. The relative density reached at 98 %. The formed scaffold will perform effective biocompatibility and high mechanical strength.

References

- [1] M. Minh, "Ceramic Fuel Cells", *Journal of the American Ceramic Society*, 76 (1993) 563-588.
- [2] S. Kirihara, L. Noritake, S. Tasaki, H. Abe, "Smart Processing of Solid Electrolyte Dendrites with Ordered Porous Structures for Fuel Cell Miniaturization", *Ceramic Interconnect and Ceramic Microsystems Technology*, 7 (2001) 17-22.
- [3] S. Kirihara, K. Noritake, S. Tasaki, H. Abe, "Smart Materials Tectonics: Development of Solid Electrolyte Dendrites", *Proceeding of the 19th Annual International Conference on Composites / Nano Engineering*, 19 (2011) 579-580.
- [4] S. Kirihara, "Terahertz Wave Control Using Ceramic Photonic Crystals with Diamond Structure Including Plane Defects Fabricated by Micro Stereolithography", *International Journal of Applied Ceramic Technology*, 6 (2009) 41-44.
- [5] S. Kirihara, "Development of Photonic and Thermodynamic Crystals Conforming to Sustainability Conscious Materials Tectonics", *WIT Transactions on Ecology and Environment*, 154 (2011) 103-114.
- [6] V. Karageorgiou, D. Kaplan, "Porosity of 3D Biomaterial Scaffolds and Osteogenesis", *Biomaterials*, 26 (2005) 5474-5491.
- [7] A. L. Olivares, E. Marsal, J. A. Planell, D. Lacroix, "Finite Element Study of Scaffold Architecture Design and Culture Conditions for Tissue Engineering", *Biomaterials*, 30 (2009) 6142-6149.